The Role of Propagative Capillary Waves in Droplet Formation from Ligament

J. Shinjo[*1], S. Matsuyama[1], Y. Mizobuchi[1], S. Ogawa[1] and A. Umemura[2]
[1]Numerical Analysis Group, Japan Aerospace Exploration Agency
Tokyo Japan
[2]Department of Aerospace Engineering, Nagoya University
Nagoya Japan

Abstract

A newly proposed understanding of droplet formation mechanism from a ligament considering the role of propagative capillary waves is numerically investigated in detail in a low-speed liquid jet configuration similar to the previous experiments. Two modes of pinch-off are reproduced by the present numerical simulation, and both modes can be explained by the new understanding. In the short-wave mode, a relatively large steady wave generated by the tip is locally destabilized and induces pinch-off. At the same time, shorter waves can travel much faster on the liquid column surface, so if they can reach the nozzle exit, they are reflected and elongated by the Doppler shift. These waves induce the long-wave or Rayleigh mode if the liquid column is long enough. It implies that the system has a disturbance source in itself, while external unknown disturbances are usually given in the classical Rayleigh analysis setup. By changing flow parameters such as the Weber and Ohnesorge numbers, the interaction of adjacent wave crests is dynamically observed and this is a clear indication of wave dynamics. In this study, it is shown that two pinch-off modes can be consistently explained by considering the propagative capillary waves.

Introduction

In turbulent atomization, there are multi-scale processes. A liquid jet core is first disturbed by the surrounding air. The surface of the liquid core becomes unstable by this aerodynamic interaction. Ligaments are then created from the surface. From these ligaments, droplets are generated. This droplet generation process is in the Weber number range of O(1), and very important in understanding the spray characteristics. Droplet creation from a ligament is equivalent to droplet pinch-off from a low-speed liquid jet, so the stability of a liquid column has been considered to explain this process. Rayleigh's analysis was the first one and the basic idea of its analysis has been used in previous research [1,2]. In the Rayleigh analysis, disturbances are assumed to be included from the beginning or given from outside and only the growth is discussed. The origin of the disturbances is not discussed and propagative waves are not included in the analysis.

Microgravity experiments by one of the authors [3] suggest a new idea that the role of propagative capillary waves is significant in actual pinch-off phenomena. As the liquid column end always exists, the tip contraction motion always creates waves on the surface that propagate upstream. Propagative waves are not unstable themselves, but the results suggest they can be easily destabilized. Two typical modes were observed in the experiments and they are called short-wave mode and long-wave mode hereafter. In the literature, the short-wave mode is related to end-pinching [4] and the long-wave mode corresponds to the classical Rayleigh mode or capillary instability [1,2]. Umemura [3,5-8] has theoretically pointed out that these two modes can be commonly explained by the destabilization of propagative capillary waves. The short-wave mode is induced by the continuous motion of a steady-state (small-wavenumber) wave from the tip that firstly compresses the liquid column and then becomes unstable to suck the liquid from the column. The existence of the tip plays an important role in this destabilization process. The long-wave mode is driven by large-wavenumber (fast-traveling) waves. Their reflection at the nozzle exit elongates the wavelength, thus these waves are destabilized.

This concept was confirmed overall in the past experiments. However, in the experiments, detailed surface motion cannot be observed. In the present study, numerical simulations are carried out to examine the role of propagative capillary waves in more detail. Furthermore, ideal settings can be made in numerical simulation. Two different flow conditions are used here to understand the droplet formation mechanism and the dominant factor in mode selection.

[*]Corresponding author, shinjo.junji@jaxa.jp

Numerical Setting and Methods

The flow setting corresponds to that of the experiments by Umemura [3]. Figure 1 shows the illustration of the flow field. The liquid is SF_6 and the surrounding gas is N_2. The liquid is injected through a round nozzle with a fixed flat velocity distribution. No external disturbances are added to the liquid flow. The liquid inflow conditions are fixed and the other boundaries (side and outflow) are treated as free out-going boundaries.

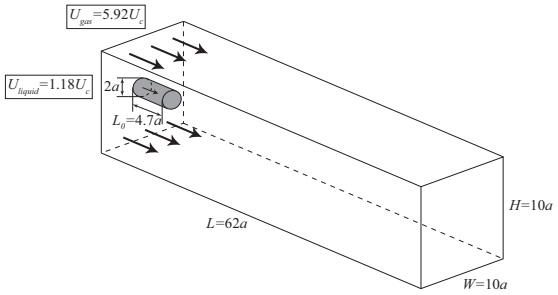

Figure 1. Numerical setup of case 1. The similar configuration is used for case 2.

Table 1 shows the flow conditions. Initially, the gas and liquid has the velocity specified in the table. The initial liquid column shape is cylinder. In case 1, the gas velocity is set higher than the liquid velocity so that the liquid column will become longer as the time passes. In case 2, the gas velocity is zero. In this case, the liquid column length is expected to become short, so the initial length is set longer. The ambient gas pressure has almost no meaning in the dynamics of pinch-off, but here changing the pressure means that the surface tension coefficient is varied accordingly. In case 2, the Ohnesorge number $Oh = \mu/\sqrt{2\rho\sigma a}$ is set smaller with a larger surface tension coefficient.

Table 1. Flow conditions

	Ambient pressure p	Nozzle diameter D=2a	Initial liquid column length L_0	Gas velocity U_g	Liquid velocity U_l
Case 1	9.1MPa	0.1mm	4.7a	0.1m/s	0.02m/s
Case 2	7.0MPa	0.1mm	16.6a	0.0m/s	0.1m/s

Liquid density ρ_l	Surface tension coefficient σ	Liquid Viscosity μ_l	Liquid Weber number $We = \rho_l U_l^2 a/\sigma$	Ohnesorge number $Oh = \mu/\sqrt{2\rho\sigma a}$
1394kg/m^3	0.02e-3N/m	9.056e-5Pa·s	1.4	0.054
1334kg/m^3	0.4e-3N/m	8.083e-5Pa·s	1.7	0.011

The governing equations are 3D incompressible Navier-Stokes equations. The expected phenomenon will be purely axisymmetric under the present flow conditions indicated in Table 1, but the numerical code is 3D for possible future extension to different conditions. Surface tension is evaluated by the Continuum Surface Force (CSF) method [9]. The numerical scheme used here is the Cubic Interpolated Pseudo-particle (CIP) method [10]. This method enables a low numerical error calculation of a flow field including a large density difference. The gas-liquid interface is tracked by the level set method [11,12]. To improve the volume conservation of the level set method, a modified version of volume-of-fluid (VOF) method called the Multi-interface Advection and Reconstruction Solver (MARS) method is combined together [13,14]. The grid points used are 6-10 million, and a grid dependency test has shown that this range of grid number is sufficient to reproduce the phenomenon considered here.

Results and Discussion

First, the effect of velocity difference was examined in advance, for example, by setting the relative gas-liquid velocity zero. The results are not shown here due to limitations in space, but under the present parameter range, the same motion by capillary waves occurred, thus the K-H shear instability was not driving the motion described below.

In the initial transient start-up of the jet, the R-T instability was suppressed by capillary wave motion, so this mechanism was not the dominant one, either.

In case 1, it is expected that two pinch-off modes appear sequentially as the time passes. Figure 2 shows the overall motion in this case. At the early stage (t<29.6), droplets are created at a short wavelength (spatial interval). This mode is called the short-wave mode. As the time passes, the long-wave mode emerges (t>34.5). These two modes can be explained by the propagative capillary waves.

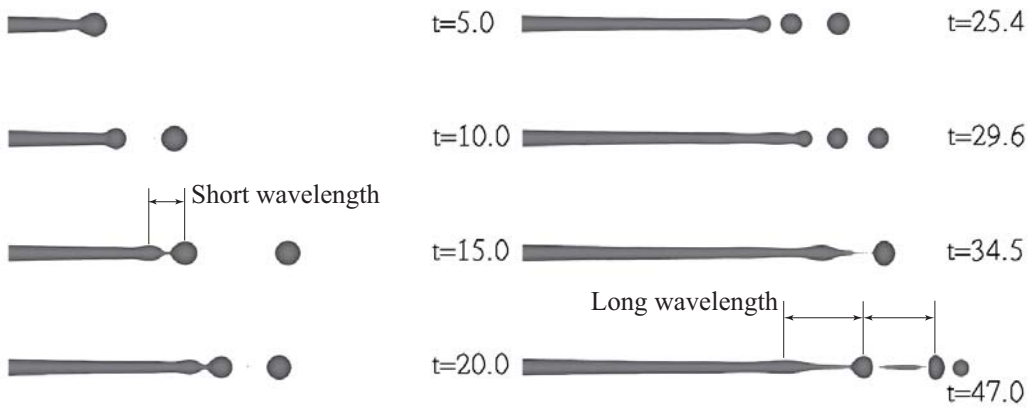

Figure 2. Overall behavior of case 1

In the short-wave mode, the dominant wavelength of pinch-off is about 3.6a where a is the radius of the nozzle exit. For droplet pinch-off to proceed, necks should be first created on the surface. Umemura [6] has shown that this interval is the wavelength of steady propagative capillary wave. The existence of the tip always emanates propagative waves toward upstream because the tip pushes the liquid upstream. These waves vary in wavelength (wavenumber) but soon converge to a dominant wavelength. The wavelength of this dominant wave is $2\pi/\sqrt{3}\,a = 3.62a$.

In pure wave propagation, these waves are not unstable. In one cycle, necks will recover and become crests, and then return again to necks. So, there should be a mechanism to destabilize these necks and it is the existence of the tip. Because the tip bulb should absorb all the liquid from upstream, its size continues to grow. As the size becomes large, the inner pressure becomes lower. This means the liquid at the first neck is absorbed further by the tip bulb, thus the first neck grows further. Finally pinch-off occurs when the surface tension in the circumferential direction exceeds that in the generating line direction. Figure 3 shows the time sequence of this motion. The color indicates the non-dimensional pressure distribution and the relative velocity to the tip is drawn together.

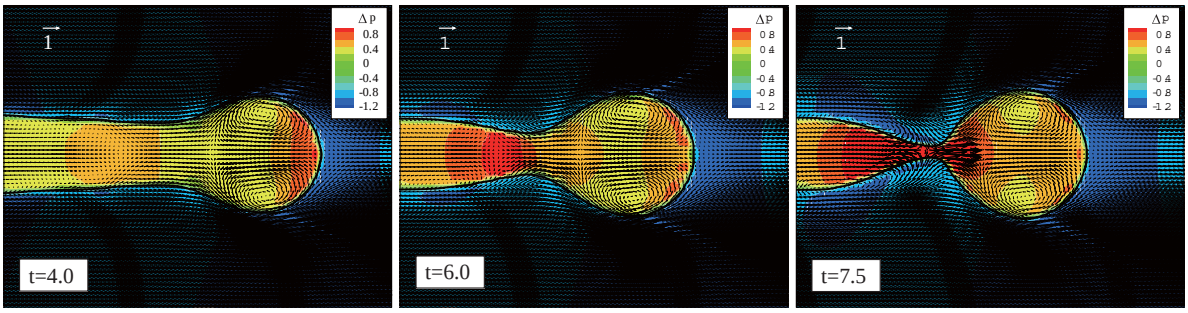

Figure 3. Neck destabilization process. Left: Initial formation of necks. The tip bulb is pushing the liquid upstream, so the pressure is high. Middle: The bulb pressure becomes low and sucks the liquid in the upstream. Right: Final motion toward pinch-off.

This short-wave mode is closed in the vicinity of the tip. Even in such a case, however, there are short wavelength (high wavenumber) waves that propagate far upstream much faster. Shinjo et al. [15] have shown that short

capillary waves propagate faster than long waves. (At the same time, short waves are more susceptible to viscous damping.) If such waves exist, they can possibly reach the nozzle exit. Figure 4 shows the root shapes at the initial stage for case 1 and a virtual case without surface tension. In the present case, there are wavy patterns on the surface that reach the nozzle exit.

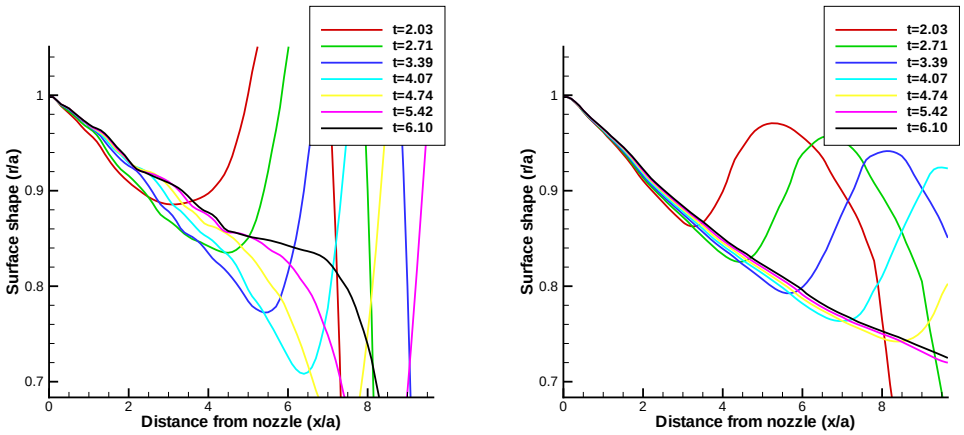

Figure 4. Root shapes for case 1 (left) and a virtual case without surface tension (right).

When these waves reach the nozzle, they must be reflected. The reflected waves become much longer by the Doppler shift, because the relative velocity between the wave propagation speed and the liquid injection velocity determines the wavelength. The reflected waves may be destabilized because they are long. This destabilization mechanism itself is the same as the Rayleigh instability mechanism. The point here is that this mode is induced by the upstream propagating waves and their reflection at the nozzle, not by any external disturbance input. As already seen in Fig. 2, the long-wave mode emerges after some time from the beginning of jet injection. This mode takes more time and more length to grow compared to the short-wave mode, thus initially only the short-wave mode appears.

Once surface waves are superposed, it becomes difficult to track each wave. However, if linear superposition is assumed, a 1D model calculation for one Fourier component considering wave propagation and the Doppler shift can clearly explain this reflection and destabilization [6-8]. Figure 5 shows the result. Four loci of waves are plotted with their amplitude growth rate Ω. At t=34, transition from pure short-wave mode to long-wave mode occurs. This timing is the same as the time when upstream traveling waves are reflected and have come back to the tip with grown amplitudes.

It is stressed again that both modes are driven by the generation of propagative capillary waves from the tip. The tip always exists, thus these modes are self-excited and self-sustained.

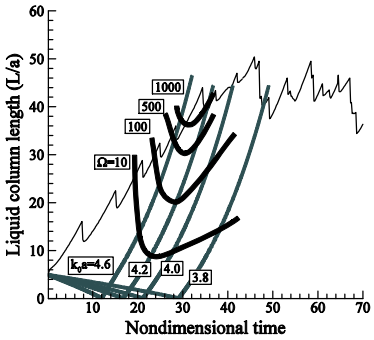

Figure 5. History of tip position by 3D simulation (saw-tooth line) and loci of wave position by 1D model calculation. Ω denotes the linear growth rate.

In case 1, the wave propagation is comparatively slow. In case 2, the Ohnesorge number is smaller, so the wave propagation is relatively faster. Next, this case is analyzed.

Figure 6 shows the history of tip position for case 2. The initial liquid column length is set longer. As is expected, the short-wave mode is dominant because the overall wave speed is faster. Before t=100, the averaged tip position moves closer to the nozzle and after t=100, it reaches a balanced state. Because the balanced liquid column length is about 10 times the radius, the long-wave mode cannot grow enough within this short column length.

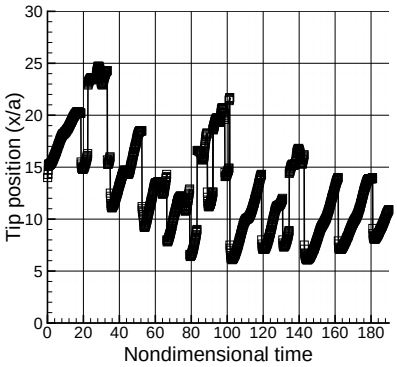

Figure 6. History of tip position for case 2. Re-collision of the liquid column and a preceding droplet temporarily increases the distance between the tip and nozzle.

A typical pinch-off cycle is shown in Fig. 7. In this case, not only the tip bulb (first crest), but the second and third crests also have a dynamic effect on the motion. In the initial stage, there are clear wavy shapes on the surface. At t=153.7, the rotating motion can be observed near the first neck and the second neck. This means wave propagation is dominant. But the liquid column shape is not symmetric, so the balance between the adjacent parts determines the following motion. At t=157.0, the first neck becomes destabilized as the tip pressure decreases. The liquid moves away from the first neck. At the same time, the downstream (right) half of the second crest tries to push the liquid toward upstream and convey a wave, because the local curvature is high and it behaves just like a tip bulb in the initial stage. This motion at the very first stage recovers the first neck slightly and then enhances the first neck growth. The second neck is recovered by this motion, so at t=160.2, the second neck has recovered much and the second and third crests seem united. Then, finally, pinch-off occurs at the first neck.

In this case, the concept of wave propagation explains the behavior. Only the short-wave mode appears and this selection can be also explained by the wave concept as described above.

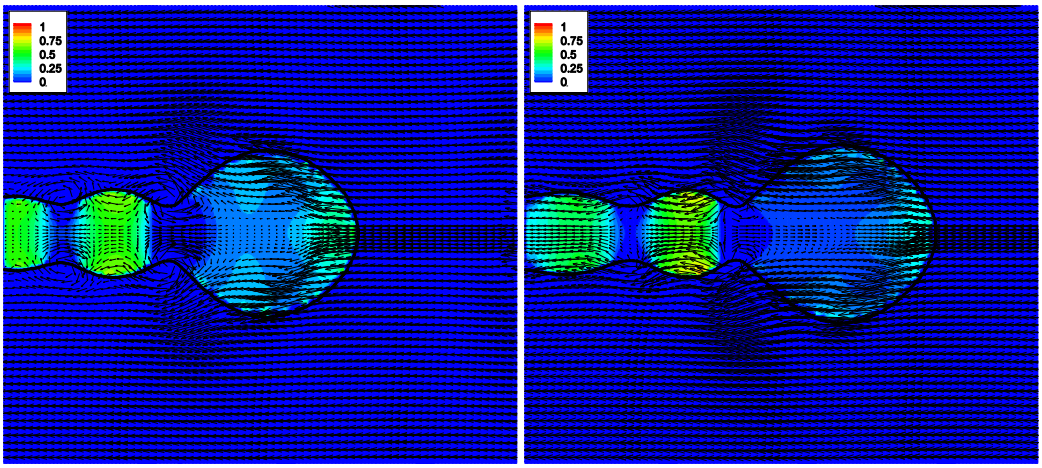

t=153.7 t=157.0

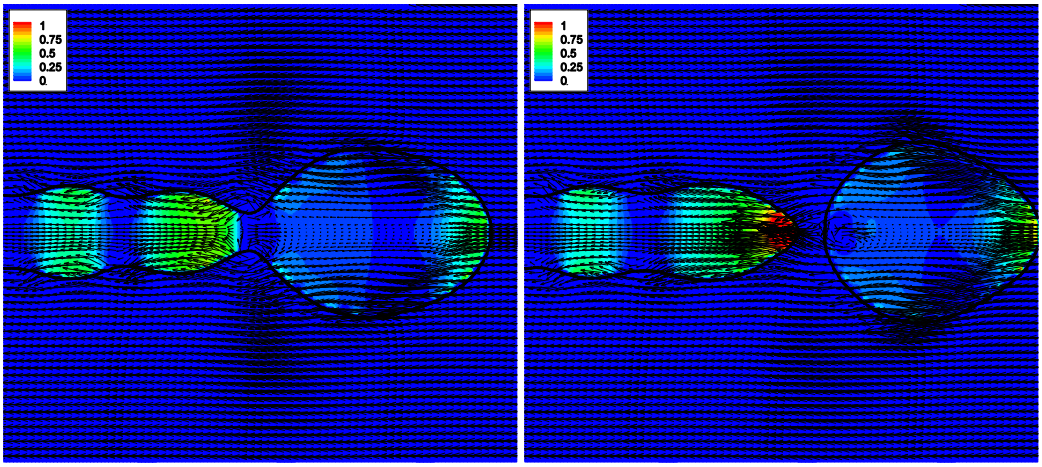

t=160.2 *t*=161.8

Figure 7. Typical motion in one cycle for case 2. The left boundary corresponds to the nozzle exit position. The relative velocity vectors are drawn with a skip for clarity.

Conclusions

Numerical simulations on droplet pinch-off have been conducted and the role of propagative capillary waves has been clarified. The ligament tip is a source of propagative capillary waves. These waves travel upstream on the liquid column surface and create necks and crests. In the tip region, soon the steady wave becomes dominant and the pinch-off spatial interval is determined by this wavelength. This steady propagative capillary wave can be naturally destabilized due to the existence of the tip and finally pinch-off occurs. It is also found that the propagative waves induce the long-wave or Rayleigh mode. Short and faster waves can reach the nozzle exit from the tip and they are reflected. The Doppler shift elongates these waves and they become convectively unstable. Thus, the two modes are driven by the wave dynamics.

The same explanation can be applied to a stronger surface tension case. In this case, not only the tip bulb, but also the second and third crests behave similarly trying to emanate propagative waves. These additional waves interact with the adjacent regions and the pinch-off process becomes more complicated. But the basic mechanism is the same and the tip region finally destabilizes the neck and leads to pinch-off. This new concept of propagative wave will be used to modify the droplet formation modeling for future spray simulations.

References

1. Rayleigh, Lord, *The Theory of Sound*, Macmillan, 1896 (reprinted by Dover 1945)
2. Lin, S. P., *Breakup of Liquid Sheets and Jets*, Cambridge University Press, 2003
3. Umemura, A. and Wakashima, Y., *Proc. Combust. Inst.*, 29, 633-640 (2002)
4. Stone, H. A. and Leal, L. G., *J Fluid Mech.*, 198, 399-427 (1989)
5. Umemura, A., *J. Japan Soc. Microgravity Appl.*, 21, 293-299 (2004)
6. Umemura, A., *J. Japan Soc. Aero. Space Sci.*, Vol. 55, No. 640, 216-223 (2007)
7. Umemura, A., *J. Japan Soc. Aero. Space Sci.*, Vol. 55, No. 640, 224-231 (2007)
8. Umemura, A., *J. Japan Soc. Aero. Space Sci.*, Vol. 55, No. 643, 359-366 (2007)
9. Brackbill, J. U., Kothe, D. B. and Zemach, C., *J. Comput. Phys.*, 100, 335-354 (1992)
10. Takewaki, H., Nishiguch, A. and Yabe, T., *J. Comput. Phys.*, 61, 261-268 (1985)
11. Sussman, M., Smereka, P. and Osher, S., *J. Comput. Phys.*, 114, 146-159 (1994)
12. Sussman, M. and Puckett, E. G., *J. Comput. Phys.*, 162, 301–337 (2000)
13. Kunugi, T., *J. Japan Soc. Mech. Eng. (series B)*, Vol.63, No.609, 1576-1584 (1997)
14. Himeno, T. and Watanabe, T., *J. Japan Soc. Mech. Eng. (series B)*, Vol.69, No.687, 2400-2407 (2003)
15. Shinjo, J., Ogawa, S. and Umemura, A., *J. Japan Soc. Aero. Space Sci.*, Vol.55, No.641, 273-281 (2007)